

Chiral charge order in $1T$ -TiSe₂: importance of lattice degrees of freedom

B. Zenker¹, H. Fehske¹, H. Beck², C. Monney³, and A. R. Bishop⁴

¹*Institut für Physik, Ernst-Moritz-Arndt-Universität Greifswald, D-17489 Greifswald, Germany*

²*Département de Physique and Fribourg Center for Nanomaterials, Université de Fribourg, CH-1700 Fribourg, Switzerland*

³*Fritz-Haber-Institut der Max Planck Gesellschaft, Faradayweg 4-6, 14195 Berlin, Germany*

⁴*Theory, Simulation, and Computation Directorate, Los Alamos National Laboratory, Los Alamos, New Mexico 87545, USA*

(Dated: March 24, 2019)

We address the question of the origin of the recently discovered chiral property of the charge-density-wave phase in $1T$ -TiSe₂ which so far lacks a microscopic understanding. We argue that the lattice degrees of freedom seems to be crucial for this novel phenomenon. We motivate a theoretical model that takes into account one valence and three conduction bands, a strongly screened Coulomb interaction between the electrons, as well as the coupling of the electrons to a transverse optical phonon mode. The Falicov-Kimball model extended in this way possesses a charge-density-wave state at low temperatures, which is accompanied by a periodic lattice distortion. The charge ordering is driven by a lattice deformation and electron-hole pairing (excitonic) instability in combination. We show that in addition an explicit phonon-phonon interaction must be taken into account to achieve a stable chiral charge order. The chiral property is exhibited in the ionic displacements. Exploring the interplay between electron-electron interaction and the electron-phonon coupling in the whole parameter regime, we provide the ground-state phase diagram of the model and give an estimate of the electron-electron and electron-phonon interaction constants for $1T$ -TiSe₂.

PACS numbers: 71.45.Lr, 71.27.+a, 63.20.kk, 71.35.Lk, 71.38.-k

I. MOTIVATION

Charge-density-waves (CDWs) brought about by electron-phonon¹ or electron-electron² interactions are broken-symmetry ground states, typically of low-dimensional (D) solids with anisotropic properties.³ A prominent material exhibiting such a periodic real-space modulation of its charge density is the transition-metal dichalcogenide $1T$ -TiSe₂. This quasi-2D system undergoes a structural phase transition at about 200 K, at which a commensurate $2 \times 2 \times 2$ superstructure accompanied by a CDW develops.⁴ Thereby the CDW features three coexisting components and, for this reason, is denoted as triple CDW. Although the charge ordered phase in $1T$ -TiSe₂ has been a matter of intensive research for more than three decades, the driving force behind the phase transition has not been identified conclusively.

Recent experiments on $1T$ -TiSe₂, pointing to a very unusual chiral property of the CDW, have reinforced the interest in this problem.^{5,6} An object exhibits chirality if it cannot be mapped on its mirror image solely by rotations and translations. For a CDW phase characterized by a scalar quantity such chirality has not been detected before. The scanning tunneling microscopy measurements performed by Ishioka and co-workers, however, show that the amplitude of the tunneling current modulates differently along the CDW unit vectors in $1T$ -TiSe₂.⁵ Since the tunneling-current amplitude directly measures the local electron density, the charge density modulates differently along the three unit vectors. As a result the material in its low-temperature phase will not exhibit a three-fold symmetry as suggested by the triangular lattice structure. The Fourier transformation

of the scanning tunneling microscopy data demonstrates a triple CDW as well as a different charge modulation along each CDW component with the respective ordering vector Q_α , $\alpha = 1, 2, 3$.⁵ If one orders the triple-CDW components according to their charge modulation amplitude in ascending order, in a sense a direction is induced and the triple CDW exhibits chirality because the mirror symmetry is broken, in contrast to usual CDWs,⁶ see the schematic representation by Fig. 1. Note that clockwise and anticlockwise chiral CDWs were found in the same sample, suggesting that these states are degenerate. This

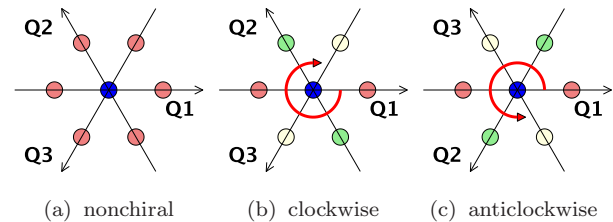


FIG. 1. (color online) Electron-density pattern for a triangular lattice in case of (a) a nonchiral CDW or (b,c) chiral CDWs. Filled circles picture the value of the charge densities, where equal colors mark equal densities. For the nonchiral CDW shown in (a) the density modulation along the ordering vectors Q_1 , Q_2 , and Q_3 is equal. Reflection along an ordering vector yields the same density pattern, i.e., mirror symmetry exists. The situation changes for a chiral CDW. A clockwise CDW (red arrow) is illustrated in (b). Now reflection along Q_1 yields the situation depicted in panel (c). Obviously the pattern (c) describes an anticlockwise CDW: That is, for a chiral CDW mirror symmetry is broken.

two-fold symmetry is corroborated by optical polarimetry measurements.⁵ Ishioka and co-workers furthermore noticed that the experimental data can be reproduced by a charge density modulation of the form

$$n_i(\mathbf{Q}_\alpha) = A \cos(\mathbf{Q}_\alpha \mathbf{R}_i + \theta_\alpha), \quad (1)$$

where A is the modulation amplitude and θ_α are initial phases.⁵ For a chiral CDW to exist the phases of the CDW components must differ, i.e., $\theta_1 \neq \theta_2 \neq \theta_3$.

From a theoretical point of view the chiral CDW in $1T$ -TiSe₂ was addressed by a Landau-Ginzburg approach.^{7,8} Thereby the relative phases of the CDW order parameters were obtained by minimizing the free energy functional. Two CDW transitions were found with decreasing temperature: Firstly a standard (nonchiral) CDW appears, and subsequently a chiral CDW emerges, i.e., $T_{\text{nonchiral CDW}} > T_{\text{chiral CDW}}$. Within the CDW phase three distinct orbital sectors are occupied, leading to an orbital-ordered state and three interacting lattice displacement waves (with different polarizations).

An open issue is the microscopic mechanism driving the CDW transition. Basically two scenarios were discussed in the literature, where the charge order results from purely electronic, respectively electron-lattice, correlations. Angle-resolved photoemission spectroscopy data reveal a relatively large transfer of spectral weight from the original bands to the back-folded bands (due to the CDW transition), compared with the small ionic displacement. This suggests an electronic mechanism within the excitonic insulator (EI) scenario.^{9,10} A corresponding tight-binding calculation estimates the amplitude of the lattice deformation caused by an EI instability to be of the same order as the measured one.¹¹ The gradual suppression of the CDW phase by changing solely electronic properties by intercalation with S or Te further corroborates the EI concept.¹² Most convincingly, time-resolved photoemission spectroscopy reveals an extremely fast response of the CDW to external light pulses which favors an electronic mechanism.¹³ Alternatively, the coupling to the lattice degrees of freedom may drive the CDW transition, e.g., by a cooperative Jahn-Teller effect.^{14,15} Here the particular form of the phonon dispersion and the softening of transverse optical phonon modes were elaborated within a tight-binding approach and found to agree with the experimental results.^{16–19} The same holds for an ab-initio approach²⁰ to a Jahn-Teller effect. Likewise the onset of superconductivity by applying pressure may be understood within a phonon-driven CDW scenario.²¹ Since some properties of the CDW in $1T$ -TiSe₂ can be understood by the excitonic condensation of electron-hole pairs and others by the instability of a phonon mode, a combined scenario has been proposed.²²

As yet it is unclear whether the chiral property of the CDW favors the electronic or lattice scenario, or a combination of both. In the present work, this issue is addressed amongst others. We start by investigating the CDW from an EI perspective. The corresponding mean-field approach for an extended Falicov-Kimball model is

presented in Sec. II A. We show that the EI scenario is insufficient to explain a stable chiral CDW. We proceed by including the lattice degrees of freedom. It turns out that, besides an electron-phonon coupling, the phonon-phonon interaction has to be taken into account in order to stabilize chiral charge order. This is elaborated in Sec. II B. The self-consistency equations for the CDW and EI order parameters are derived in Sec. II C. The CDW state is characterized analytically in Sec. II D. Section III contains our main (numerical) results. Here we give the functional dependences of the EI order parameter and the lattice distortion on the model parameters and temperature, derive the ground-state phase diagram, and estimate the interaction constants for $1T$ -TiSe₂. In Sec. IV, we summarize and conclude.

II. MODEL AND THEORETICAL APPROACH

A. Electronic degrees of freedom

1. Band structure

Since the electronic properties of $1T$ -TiSe₂ are dominated by the electrons near the Fermi energy, in what follows we only take into account the top valence band and the lower conduction band. The maximum of the valence band is located at the Γ -point. The conduction band exhibits minima at the three L -points, see Fig. 2. To facilitate the notation, we artificially split the conduc-

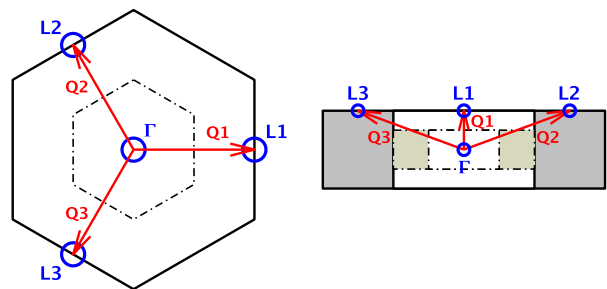


FIG. 2. (color online) First Brillouin zone (BZ) of $1T$ -TiSe₂ with high symmetry points in the normal phase (solid line) and in the CDW phase (dot-dashed line). Red arrows show the CDW ordering vectors. Left panel: projection onto the xy -plane, right panel: projection onto the yz -plane.

tion band into three symmetry-equivalent bands indexed by α , each having one minimum at the point L_α . The band dispersions of these three conduction bands mimics the true band structure close to the L -points.¹⁰ Figure 3 illustrates the situation close to the Fermi level. Then the free electron part is written as

$$H_e = \sum_{\mathbf{k}} \varepsilon_{\mathbf{k}f} f_{\mathbf{k}}^\dagger f_{\mathbf{k}} + \sum_{\mathbf{k}, \alpha} \varepsilon_{\mathbf{k}\alpha} c_{\mathbf{k}\alpha}^\dagger c_{\mathbf{k}\alpha}, \quad (2)$$

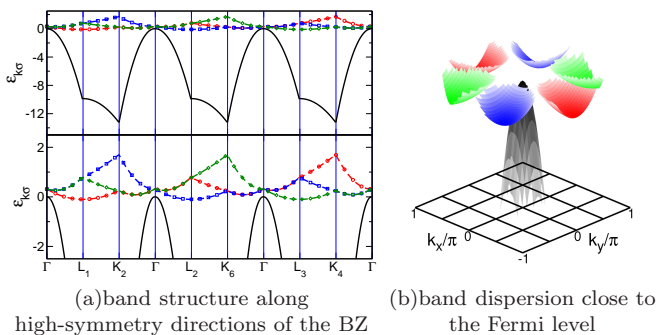


FIG. 3. (color online) Model band structure in the normal phase. The valence band is colored in black and the conduction bands are colored red, blue, and green.

where $f_{\mathbf{k}}^{(\dagger)}$ annihilates (creates) an electron in the valence band with momentum \mathbf{k} and $c_{\mathbf{k}\alpha}^{(\dagger)}$ annihilates (creates) an electron in the conduction band with momentum \mathbf{k} and band index α . The corresponding valence-band dispersion and the conduction-band dispersions are denoted as $\varepsilon_{\mathbf{k}f}$ and $\varepsilon_{\mathbf{k}\alpha}$. They will be specified in Sec. III A. The spin of the electrons is neglected.

Taking the band structure and a band filling factor $n = 1/4$ into account, $1T$ -TiSe₂ resides in the vicinity of a semimetal-semiconductor transition, cf. Fig 3. Accordingly the chemical potential μ is determined by

$$n_f + \sum_{\alpha} n_{\alpha} = 1, \quad (3)$$

where

$$n_f = \frac{1}{N} \sum_{\mathbf{k}} \langle n_{\mathbf{k}}^f \rangle = \frac{1}{N} \sum_{\mathbf{k}} \langle f_{\mathbf{k}}^{\dagger} f_{\mathbf{k}} \rangle, \quad (4)$$

$$n_{\alpha} = \frac{1}{N} \sum_{\mathbf{k}} \langle n_{\mathbf{k}}^{\alpha} \rangle = \frac{1}{N} \sum_{\mathbf{k}} \langle c_{\mathbf{k}\alpha}^{\dagger} c_{\mathbf{k}\alpha} \rangle. \quad (5)$$

Here N denotes the total number of lattice sites.

Regarding the isotropy (anisotropy) of the valence (conduction) band(s) the Fermi surface of $1T$ -TiSe₂ is only poorly nested,¹⁵ which rules out a nesting mechanism for the CDW formation even in a simplified 2D setting.

2. Electron-electron interaction

Due to the strong screening of the Coulomb interaction in $1T$ -TiSe₂,²³ we assume a local electron-electron interaction,

$$H_{e-e} = \frac{U_{cc}}{N} \sum_{\mathbf{k}, \mathbf{k}', \mathbf{q}} \sum_{\alpha} \sum_{\beta > \alpha} c_{\mathbf{k}+\mathbf{q}\alpha}^{\dagger} c_{\mathbf{k}\alpha} c_{\mathbf{k}'\beta}^{\dagger} c_{\mathbf{k}'+\mathbf{q}\beta} + \frac{U_{fc}}{N} \sum_{\mathbf{k}, \mathbf{k}', \mathbf{q}} \sum_{\alpha} f_{\mathbf{k}+\mathbf{q}}^{\dagger} f_{\mathbf{k}} c_{\mathbf{k}'\alpha}^{\dagger} c_{\mathbf{k}'+\mathbf{q}\alpha}, \quad (6)$$

where U_{cc} denotes the Coulomb repulsion among the conduction electrons. The on-site Coulomb interaction U_{fc} between valence and conduction band electrons determines the distribution of electrons between these “subsystems” and therefore may drive a valence transition, as observed, e.g., in heavy fermion and intermediate-valence Tm[Se,Te] compounds.^{24,25} If the total electronic model contains an explicit hybridization between f and c electrons^{26,27} or, as in our case, dispersive c and f bands,²⁸ coherence between c and f particles can develop. Then U_{fc} may lead to a pairing of c -band electrons and f -band holes, i.e., to the formation of excitons and, provided a large enough number of excitons is created, a subsequent spontaneous condensation of these composite quasiparticles may develop. In real systems this excitonic instability is expected to occur, when semimetals with very small band overlap or semiconductors with very small band gap are cooled to extremely low temperatures.^{29,30} The excitonic condensate then typifies a macroscopic phase-coherent insulating state, the EI, which separates the semimetal from the insulator.^{31,32} From a theoretical point of view, Falicov-Kimball-type models seem to be the most promising candidates for realizing collective excitonic phases. This holds particularly for the generic two-band extended Falicov-Kimball model (EFKM), where an EI ground state has been proven to exist in 1D and 2D by constrained-path Monte Carlo simulations.^{28,33} Subsequent Hartree-Fock, slave-boson and projector-based renormalization techniques yield the 2D EFKM ground-state phase diagram in even quantitative accordance with unbiased Monte Carlo data,³⁴⁻⁴² supporting the applicability of these analytical approaches also in 3D and for more complicated situations.

The electronic part of our Hamiltonian,

$$H_{\text{mEFKM}} = H_e + H_{e-e}, \quad (7)$$

can be viewed as a multiband extended Falicov-Kimball model (mEFKM). We note that the mEFKM was studied previously and has been shown to reproduce the angle-resolved photoemission spectroscopy data for $1T$ -TiSe₂ at temperatures below the critical temperature^{9,10,43-45}, as well as above but close to the critical temperature.^{23,46}

We note that the mEFKM exhibits a particular U(1) symmetry. This can be seen by applying the unitary transformation $U_{\varphi, \alpha} = e^{i\varphi S_{\alpha}}$ with $S_{\alpha} = \frac{1}{2} \sum_i (f_i^{\dagger} f_i - c_{i\alpha}^{\dagger} c_{i\alpha})$. The operators $f_i^{(\dagger)}$ and $c_{i\alpha}^{(\dagger)}$ annihilate (create) an electron at Wannier site i . Obviously we have

$$H_{\text{mEFKM}} = U_{\varphi, \alpha} H_{\text{mEFKM}} U_{\varphi, \alpha}^{\dagger}. \quad (8)$$

This symmetry leads to a degeneracy between chiral and nonchiral CDWs (see below).

To proceed, we perform a Hartree-Fock decoupling of

the electron-electron interaction terms:

$$\frac{U_{cc}}{N} \sum_{\mathbf{k}, \mathbf{k}', \mathbf{q}} \sum_{\alpha} \sum_{\beta > \alpha} c_{\mathbf{k}+\mathbf{q}\alpha}^{\dagger} c_{\mathbf{k}\alpha} c_{\mathbf{k}'\beta}^{\dagger} c_{\mathbf{k}'+\mathbf{q}\beta} \rightarrow$$

$$U_{cc} \sum_{\mathbf{k}} \sum_{\alpha} \sum_{\beta \neq \alpha} c_{\mathbf{k}\alpha}^{\dagger} c_{\mathbf{k}\alpha} n_{\beta} - NU_{cc} \sum_{\alpha} \sum_{\beta > \alpha} n_{\alpha} n_{\beta}, \quad (9)$$

$$\frac{U_{fc}}{N} \sum_{\mathbf{k}, \mathbf{k}', \mathbf{q}} \sum_{\alpha} f_{\mathbf{k}+\mathbf{q}}^{\dagger} f_{\mathbf{k}} c_{\mathbf{k}'\alpha}^{\dagger} c_{\mathbf{k}'+\mathbf{q}\alpha} \rightarrow$$

$$U_{fc} \sum_{\alpha} n_{\alpha} \sum_{\mathbf{k}} f_{\mathbf{k}}^{\dagger} f_{\mathbf{k}} + U_{fc} n_f \sum_{\mathbf{k}, \alpha} c_{\mathbf{k}\alpha}^{\dagger} c_{\mathbf{k}\alpha}$$

$$- NU_{fc} n_f \sum_{\alpha} n_{\alpha} - \sum_{\alpha} \Delta_{\mathbf{Q}\alpha} \sum_{\mathbf{k}} c_{\mathbf{k}+\mathbf{Q}\alpha}^{\dagger} f_{\mathbf{k}}$$

$$- \sum_{\alpha} \Delta_{\mathbf{Q}\alpha}^* \sum_{\mathbf{k}} f_{\mathbf{k}}^{\dagger} c_{\mathbf{k}+\mathbf{Q}\alpha} + \frac{N}{U_{fc}} |\Delta_{\mathbf{Q}\alpha}|^2. \quad (10)$$

Here we introduced the EI order parameter functions

$$\Delta_{\mathbf{Q}\alpha} = \frac{U_{fc}}{N} \sum_{\mathbf{k}} \langle f_{\mathbf{k}}^{\dagger} c_{\mathbf{k}+\mathbf{Q}\alpha} \rangle, \quad (11)$$

$$\Delta_{\mathbf{Q}\alpha}^* = \frac{U_{fc}}{N} \sum_{\mathbf{k}} \langle c_{\mathbf{k}+\mathbf{Q}\alpha}^{\dagger} f_{\mathbf{k}} \rangle. \quad (12)$$

Since the experiments on $1T$ -TiSe₂ suggest that the spontaneous hybridization of the valence band with one of the three conduction bands is the dominant effect of the electron-electron interaction,⁹ in deriving Eq. (10), we neglected all terms that mix different conduction bands.

The resulting decoupled Hamiltonian takes the form

$$\bar{H}_{\text{mEFKM}} = \sum_{\mathbf{k}} \bar{\varepsilon}_{\mathbf{k}f} f_{\mathbf{k}}^{\dagger} f_{\mathbf{k}} + \sum_{\mathbf{k}, \alpha} \bar{\varepsilon}_{\mathbf{k}\alpha} c_{\mathbf{k}\alpha}^{\dagger} c_{\mathbf{k}\alpha}$$

$$- \sum_{\mathbf{k}, \alpha} \Delta_{\mathbf{Q}\alpha} c_{\mathbf{k}+\mathbf{Q}\alpha}^{\dagger} f_{\mathbf{k}} - \sum_{\mathbf{k}, \alpha} \Delta_{\mathbf{Q}\alpha}^* f_{\mathbf{k}}^{\dagger} c_{\mathbf{k}+\mathbf{Q}\alpha}$$

$$- NU_{fc} n_f \sum_{\alpha} n_{\alpha} - NU_{cc} \sum_{\alpha} \sum_{\beta > \alpha} n_{\alpha} n_{\beta}$$

$$+ \frac{N}{U_{fc}} \sum_{\alpha} |\Delta_{\mathbf{Q}\alpha}|^2, \quad (13)$$

with shifted f and c band dispersions:

$$\bar{\varepsilon}_{\mathbf{k}f} = \varepsilon_{\mathbf{k}f} + U_{fc} \sum_{\alpha} n_{\alpha}, \quad (14)$$

$$\bar{\varepsilon}_{\mathbf{k}\alpha} = \varepsilon_{\mathbf{k}\alpha} + U_{fc} n_f + U_{cc} \sum_{\beta \neq \alpha} n_{\beta}. \quad (15)$$

The EI low-temperature phase is characterized by non-vanishing expectation values $\langle f_{\mathbf{k}}^{\dagger} c_{\mathbf{k}+\mathbf{Q}\alpha} \rangle$, $\langle c_{\mathbf{k}+\mathbf{Q}\alpha}^{\dagger} f_{\mathbf{k}} \rangle$, which cause a correlation gap in the excitation spectrum. The mean local electron density in the EI phase is

$$n_i = 1 + \frac{2}{N} \sum_{\mathbf{k}, \alpha} |\langle c_{\mathbf{k}+\mathbf{Q}\alpha}^{\dagger} f_{\mathbf{k}} \rangle| \cos(\mathbf{Q}_{\alpha} \mathbf{R}_i + \theta_{\alpha}), \quad (16)$$

where

$$\frac{1}{N} \sum_{\mathbf{k}} \langle c_{\mathbf{k}+\mathbf{Q}\alpha}^{\dagger} f_{\mathbf{k}} \rangle = \frac{1}{N} \sum_{\mathbf{k}} |\langle c_{\mathbf{k}+\mathbf{Q}\alpha}^{\dagger} f_{\mathbf{k}} \rangle| e^{i\theta_{\alpha}} = \frac{\Delta_{\mathbf{Q}\alpha}^*}{U_{fc}}. \quad (17)$$

Comparing Eq. (16) with relation (1) we recognize the amplitude of the charge density modulation as the modulus of the hybridization function $\sum_{\mathbf{k}} \langle c_{\mathbf{k}+\mathbf{Q}\alpha}^{\dagger} f_{\mathbf{k}} \rangle$. Likewise we can identify the initial phases θ_{α} in the density modulation as the phases of the hybridization functions (which coincide with the phases of the EI order parameters).

Note that previous theoretical studies of the mEFKM^{10,11} did not include the phase differences of the θ_{α} , which will be essential for the establishment of a chiral CDW.⁵⁻⁸ If one is not concerned with the chiral CDW problem, disregarding the phases θ_{α} seems to be justified since the U(1) symmetry of the mEFKM prevents the appearance of a stable chiral CDW anyway. We show this by analyzing the behavior of the electron operators under the unitary transformation $U_{\varphi, \alpha}$: $\tilde{c}_{i\alpha}^{(\dagger)} = U_{\varphi, \alpha} c_{i\alpha}^{(\dagger)} U_{\varphi, \alpha}^{\dagger}$ and $\tilde{f}_i^{(\dagger)} = U_{\varphi, \alpha} f_i^{(\dagger)} U_{\varphi, \alpha}^{\dagger}$. The hybridization functions (in real space) then transform as $\langle c_{i\alpha}^{\dagger} f_i \rangle e^{i\mathbf{Q}_{\alpha} \mathbf{R}_i} = e^{-i\varphi} \langle \tilde{c}_{i\alpha}^{\dagger} \tilde{f}_i \rangle e^{i\mathbf{Q}_{\alpha} \mathbf{R}_i}$. That is, the phases θ_{α} can be controlled by the unitary transformation through the angles φ . However, in view of (8) the total energy is independent of the θ_{α} . Hence these phases can be chosen arbitrarily and there is no mechanism that stabilizes a given phase difference. Therefore the mEFKM is insufficient to describe a chiral CDW in $1T$ -TiSe₂. In the following we will demonstrate that the coupling of the electrons to the lattice degrees of freedom can break the U(1)-symmetry of the mEFKM and consequently can stabilize a chiral CDW.

B. Lattice degrees of freedom

1. Electron-phonon coupling

For $1T$ -TiSe₂ there are experimental and theoretical evidences that the weak periodic lattice distortion observed comes from a softening of a transverse optical phonon mode.¹⁶⁻²⁰ Of particular importance in this respect is the BZ boundary phonon that connects the Γ - and L_{α} -points. The valence-band states at the Γ -point and the conduction-band states at the L_{α} -points are closest to the Fermi energy and, for momentum conservation reasons, the transfer (excitation) of an electron from Γ to L_{α} should be accompanied by the creation of a phonon with momentum $-\mathbf{Q}_{\alpha}$. Hence we assume a simplified single-mode electron-phonon interaction that contains only f - c_{α} band-mixing terms (cf. Ref. 11):

$$H_{\text{e-ph}} = \frac{1}{\sqrt{N}} \sum_{\mathbf{k}, \mathbf{q}} \sum_{\alpha} \left[g_{\mathbf{q}}^{f\alpha} (b_{\mathbf{q}}^{\dagger} + b_{-\mathbf{q}}) f_{\mathbf{k}}^{\dagger} c_{\mathbf{k}+\mathbf{q}\alpha} \right.$$

$$\left. + (g_{\mathbf{q}}^{f\alpha})^* (b_{-\mathbf{q}}^{\dagger} + b_{\mathbf{q}}) c_{\mathbf{k}+\mathbf{q}\alpha}^{\dagger} f_{\mathbf{k}} \right]. \quad (18)$$

284 Here the operator $b_{\mathbf{q}}^{(\dagger)}$ describes the annihilation (cre-
 285 ation) of a phonon carrying momentum \mathbf{q} , and $g_{\mathbf{q}}^{f\alpha}$ de-
 286 notes the electron-phonon coupling constant. The Hamil-
 287 tonian (18) can be derived microscopically following the
 288 approach in Ref. 47. Most notably the electron-phonon
 289 coupling (18) breaks the U(1) symmetry of the mEFKM,
 290 i.e., the arbitrariness with respect to the phases θ_{α} is
 291 eliminated.

2. Phonon-phonon interaction

293 Within the harmonic approximation, the Hamiltonian
 294 for the (noninteracting) phonons reads⁴⁸

$$H_{\text{ph}} = \sum_{\mathbf{q}} \hbar\omega(\mathbf{q}) b_{\mathbf{q}}^{\dagger} b_{\mathbf{q}}, \quad (19)$$

295 where $\omega(\mathbf{q})$ is the bare phonon frequency. A coupling be-
 296 tween the lattice vibrations results from the anharmonic
 297 contributions in the expansion of the potential for the
 298 ions.⁴⁹ As we will see below, such an explicit phonon-
 299 phonon interaction will be necessary to stabilize the chi-
 300 ral CDW phase. Here we will take into account only
 301 terms of cubic and quartic order in the lattice displace-
 302 ment. Then we obtain

$$\begin{aligned} H_{\text{ph-ph}} &= \frac{1}{\sqrt{N}} \sum_{\mathbf{q}_1, \mathbf{q}_2, \mathbf{q}_3} B(\mathbf{q}_1, \mathbf{q}_2, \mathbf{q}_3) (b_{\mathbf{q}_1}^{\dagger} + b_{-\mathbf{q}_1}) \\ &\quad \times (b_{\mathbf{q}_2}^{\dagger} + b_{-\mathbf{q}_2}) (b_{\mathbf{q}_3}^{\dagger} + b_{-\mathbf{q}_3}) \\ &\quad + \frac{1}{N} \sum_{\mathbf{q}_1, \mathbf{q}_2, \mathbf{q}_3, \mathbf{q}_4} D(\mathbf{q}_1, \mathbf{q}_2, \mathbf{q}_3, \mathbf{q}_4) (b_{\mathbf{q}_1}^{\dagger} + b_{-\mathbf{q}_1}) \\ &\quad \times (b_{\mathbf{q}_2}^{\dagger} + b_{-\mathbf{q}_2}) (b_{\mathbf{q}_3}^{\dagger} + b_{-\mathbf{q}_3}) (b_{\mathbf{q}_4}^{\dagger} + b_{-\mathbf{q}_4}). \quad (20) \end{aligned}$$

303 The explicit expressions of $B(\mathbf{q}_1, \mathbf{q}_2, \mathbf{q}_3)$ and
 304 $D(\mathbf{q}_1, \mathbf{q}_2, \mathbf{q}_3, \mathbf{q}_4)$ are lengthy. We only note the
 305 symmetry relations

$$B(-\mathbf{q}_1, -\mathbf{q}_2, -\mathbf{q}_3) = B^*(\mathbf{q}_1, \mathbf{q}_2, \mathbf{q}_3), \quad (21)$$

$$D(-\mathbf{q}_1, -\mathbf{q}_2, -\mathbf{q}_3, -\mathbf{q}_4) = D^*(\mathbf{q}_1, \mathbf{q}_2, \mathbf{q}_3, \mathbf{q}_4), \quad (22)$$

306 and point out the constraints

$$B(\mathbf{q}_1, \mathbf{q}_2, \mathbf{q}_3) \propto \delta_{\mathbf{q}_1 + \mathbf{q}_2 + \mathbf{q}_3, \mathbf{G}}, \quad (23)$$

$$D(\mathbf{q}_1, \mathbf{q}_2, \mathbf{q}_3, \mathbf{q}_4) \propto \delta_{\mathbf{q}_1 + \mathbf{q}_2 + \mathbf{q}_3 + \mathbf{q}_4, \mathbf{G}}. \quad (24)$$

307 Here \mathbf{G} is a reciprocal lattice vector of the undistorted
 308 lattice.

3. Frozen-phonon approach

310 We now apply the frozen-phonon approximation and
 311 calculate the lattice distortion at low temperatures. As
 312 elaborated in Refs. 17–20 the phonons causing the lat-
 313 tice displacements in 1T-TiSe₂ have the momenta \mathbf{Q}_{α}
 314 shown in Fig. 2. Their softening is inherently connected
 315 to strong electronic correlations.²³ It has been suggested

316 that the \mathbf{Q}_1 , \mathbf{Q}_2 , and \mathbf{Q}_3 phonons become soft at the
 317 same temperature;¹⁸ we therefore assume $|g_{\mathbf{Q}_1}^{f1}| = |g_{\mathbf{Q}_2}^{f2}| =$
 318 $|g_{\mathbf{Q}_3}^{f3}| = g_{\mathbf{Q}}$ (using the notation $g_{\mathbf{Q}_{\alpha}}^{f\alpha} = g_{\mathbf{Q}} e^{i\Phi_{\alpha}}$) and
 319 $\omega(\mathbf{Q}_1) = \omega(\mathbf{Q}_2) = \omega(\mathbf{Q}_3) = \omega$. A finite displacement
 320 of the ions is characterized by $\langle b_{\mathbf{Q}_{\alpha}}^{\dagger} \rangle = \langle b_{-\mathbf{Q}_{\alpha}} \rangle \neq 0$. We
 321 denote the static lattice distortions by

$$\delta_{\mathbf{Q}_{\alpha}} = \frac{2}{\sqrt{N}} g_{\mathbf{Q}} \langle b_{\mathbf{Q}_{\alpha}} \rangle e^{-i\Phi_{\alpha}} = |\delta_{\mathbf{Q}_{\alpha}}| e^{-i\phi_{\alpha}}, \quad (25)$$

$$\delta_{\mathbf{Q}_{\alpha}}^* = \frac{2}{\sqrt{N}} g_{\mathbf{Q}} \langle b_{\mathbf{Q}_{\alpha}}^{\dagger} \rangle e^{i\Phi_{\alpha}} = |\delta_{\mathbf{Q}_{\alpha}}| e^{i\phi_{\alpha}}. \quad (26)$$

322 Obviously, their phases are composed of two contribu-
 323 tions, $\phi_{\alpha} = \Phi_{\alpha} + \phi_{b\alpha}$, where Φ_{α} stems from the phase
 324 of the corresponding electron-phonon coupling constant
 325 and $\phi_{b\alpha}$ originates from the complex average value $\langle b_{\mathbf{Q}_{\alpha}} \rangle$.
 326 It will become apparent below that $\phi_{b\alpha}$ reflects the in-
 327 teraction between the different CDW components.

If we only take into account the \mathbf{Q}_{α} -phonon modes
 the cubic terms in $H_{\text{ph-ph}}$ vanish, since the finite
 z -component of the ordering vectors prevents con-
 straint (23) from being satisfied. Hence the first anhar-
 monic corrections are of quartic order. Here the geometry
 in the xy -plane is crucial. Replacing all phonon opera-
 tors by their averages, the Hamiltonian $H = H_e + H_{e-e} +$
 $H_{e-\text{ph}} + H_{\text{ph}} + H_{\text{ph-ph}}$ becomes an effective electronic
 model:

$$\begin{aligned} \bar{H} &= \bar{H}_{\text{mEFKM}} + \sum_{\mathbf{k}, \alpha} \left(\delta_{\mathbf{Q}_{\alpha}} c_{\mathbf{k} + \mathbf{Q}_{\alpha}}^{\dagger} f_{\mathbf{k}} + \delta_{\mathbf{Q}_{\alpha}}^* f_{\mathbf{k}}^{\dagger} c_{\mathbf{k} + \mathbf{Q}_{\alpha}} \right) \\ &\quad + \frac{DN}{g_{\mathbf{Q}}^4} \sum_{\alpha} \sum_{\beta > \alpha} \left[(\delta_{\mathbf{Q}_{\alpha}}^* \delta_{\mathbf{Q}_{\beta}}^*)^2 e^{-2i(\Phi_{\alpha} + \Phi_{\beta})} \right. \\ &\quad + (\delta_{\mathbf{Q}_{\alpha}} \delta_{\mathbf{Q}_{\beta}})^2 e^{2i(\Phi_{\alpha} + \Phi_{\beta})} + (\delta_{\mathbf{Q}_{\alpha}}^* \delta_{\mathbf{Q}_{\beta}})^2 e^{-2i(\Phi_{\alpha} - \Phi_{\beta})} \\ &\quad \left. + (\delta_{\mathbf{Q}_{\alpha}} \delta_{\mathbf{Q}_{\beta}}^*)^2 e^{2i(\Phi_{\alpha} - \Phi_{\beta})} \right] + \frac{\tilde{D}}{g_{\mathbf{Q}}^4} \sum_{\alpha} |\delta_{\mathbf{Q}_{\alpha}}|^4 \\ &\quad + N \sum_{\alpha} \hbar\omega \frac{|\delta_{\mathbf{Q}_{\alpha}}|^2}{4(g_{\mathbf{Q}})^2}. \quad (27) \end{aligned}$$

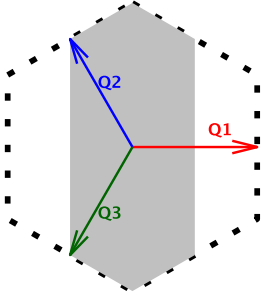
328 Here $D = D(\mathbf{Q}_{\alpha}, \mathbf{Q}_{\alpha}, \mathbf{Q}_{\beta}, \mathbf{Q}_{\beta})$ ($\beta \neq \alpha$), $\tilde{D} =$
 329 $D(\mathbf{Q}_{\alpha}, \mathbf{Q}_{\alpha}, -\mathbf{Q}_{\alpha}, -\mathbf{Q}_{\alpha})$, and we assume for simplicity
 330 that the phonon-phonon interaction constants are the
 331 same for all combinations of α and β . D and \tilde{D} are
 332 real. In Eq. (27), the term proportional to \tilde{D} , coming
 333 from the expansion of the phonon-phonon interaction,
 334 guarantees that the free energy is bounded from below
 335 within our approximations. Note that the leading terms
 336 of the phonon-phonon interaction expansion relate the
 337 phases ϕ_{α} to each other. Obviously a finite lattice dis-
 338 tortion causes a hybridization between the valence and
 339 the conduction bands. As a consequence a gap in the
 340 electronic spectrum opens, just as in the course of exci-
 341 ton condensation (cf. Eq. (13)). The corresponding local
 342 electron density is given by Eq. (16).

343 Of particular interest are the phases θ_{α} . Owing to
 344 the second term on the rhs. of Eq. (27), these phases are

345 coupled to the phases of $\delta_{\mathbf{Q}\alpha}$. Let us analyze the possible
 346 values of the phases of the static lattice distortion. We
 347 first note that every \mathbf{Q}_α is half a reciprocal lattice vector
 348 in the normal phase, i.e., $e^{2i\mathbf{Q}_\alpha\mathbf{R}_i} = 1$, where \mathbf{R}_i is a
 349 lattice vector of the undistorted lattice. Hence

$$\begin{aligned} b_{\mathbf{Q}\alpha}^\dagger &= \frac{1}{\sqrt{N}} \sum_i b_i^\dagger e^{-i\mathbf{Q}_\alpha\mathbf{R}_i} = \frac{1}{\sqrt{N}} \sum_i b_i^\dagger e^{-i\mathbf{Q}_\alpha\mathbf{R}_i + 2i\mathbf{Q}_\alpha\mathbf{R}_i} \\ &= \frac{1}{\sqrt{N}} \sum_i b_i^\dagger e^{i\mathbf{Q}_\alpha\mathbf{R}_i} = b_{-\mathbf{Q}\alpha}^\dagger. \end{aligned} \quad (28)$$

350 That is $b_{\mathbf{Q}\alpha}^\dagger$ and $b_{-\mathbf{Q}\alpha}^\dagger$ create the same phonon. This
 351 implies $\langle b_{\mathbf{Q}\alpha}^\dagger \rangle = \langle b_{-\mathbf{Q}\alpha}^\dagger \rangle = \langle b_{\mathbf{Q}\alpha} \rangle$, and $\langle b_{\mathbf{Q}\alpha} \rangle$ becomes
 352 a real number. The phase of $\delta_{\mathbf{Q}\alpha}$ is then exclusively
 353 determined by the corresponding phase of the electron-
 354 phonon coupling constant Φ_α , cf. Eqs. (25) and (26).
 355 However, since a triple CDW is not a simple superposi-
 356 tion of three single CDWs the situation is more subtle.
 357 Here the change of the periodicity of the lattice caused by
 358 one CDW component affects the formation of the other
 359 two components. To elucidate this in some more detail
 360 let us assume that phonon 1 softens at T_c , while phonon
 361 2 and phonon 3 soften at $T_c - \delta T$. As a result of the
 362 transition 1 at T_c the periodicity of the crystal changes
 363 and consequently the BZ changes too (cf. Fig. 4). The



364 FIG. 4. (color online) BZ in the normal phase (black dotted
 365 hexagon) and (artificial) BZ that would emerge if only the
 366 phonon \mathbf{Q}_1 softens (filled gray hexagon). Red, green, and
 367 blue arrows indicate the ordering vectors \mathbf{Q}_1 , \mathbf{Q}_2 , and
 368 \mathbf{Q}_3 , respectively.

365 vectors \mathbf{Q}_2 and \mathbf{Q}_3 are no longer half-reciprocal lattice
 366 vectors and Eq. (28) does not apply. Hence, at $T_c - \delta T$,
 367 $\langle b_{\mathbf{Q}_2} \rangle$ and $\langle b_{\mathbf{Q}_3} \rangle$ are complex numbers with phases that
 368 have to be determined by minimizing the free energy. For
 369 $1T$ -TiSe₂, $\delta T = 0$, but nevertheless the above discussion
 370 remains valid. That is the freedom to fix the phases of
 371 the lattice distortions in an appropriate way results from
 372 the fact that one triple-CDW component must develop
 373 in a lattice structure which is already distorted by the
 374 other two triple-CDW components.

Based on the model (27), at zero temperature, we
 can relate the phases of $\delta_{\mathbf{Q}\alpha}$ and $\sum_{\mathbf{k}} \langle c_{\mathbf{k}+\mathbf{Q}\alpha}^\dagger f_{\mathbf{k}} \rangle$. The

ground-state energy per site is

$$\begin{aligned} \frac{\bar{E}}{N} &= \frac{2}{N} \sum_{\mathbf{k}, \alpha} |\delta_{\mathbf{Q}\alpha}| |\langle c_{\mathbf{k}+\mathbf{Q}\alpha}^\dagger f_{\mathbf{k}} \rangle| \cos(\theta_\alpha - \phi_\alpha) \\ &+ \frac{4D}{g_{\mathbf{Q}}^4} \sum_{\alpha} \sum_{\beta > \alpha} |\delta_{\mathbf{Q}\alpha}|^2 |\delta_{\mathbf{Q}\beta}|^2 \cos(2\phi_\alpha - 2\Phi_\alpha) \\ &\times \cos(2\phi_\beta - 2\Phi_\beta) + \frac{\tilde{D}}{g_{\mathbf{Q}}^4} \sum_{\alpha} |\delta_{\mathbf{Q}\alpha}|^4 \\ &+ \sum_{\alpha} \hbar\omega \frac{|\delta_{\mathbf{Q}\alpha}|^2}{4(g_{\mathbf{Q}})^2} + \frac{\bar{E}_{\text{mEFKM}}}{N}. \end{aligned} \quad (29)$$

376 The first term on the rhs. of Eq. (29) is minimized with

$$\theta_\alpha - \phi_\alpha = \pi + s \cdot 2\pi, \quad s = 0, 1, 2, \dots \quad (30)$$

377 We find that the phases θ_α are locked to $\phi_\alpha + (2s + 1)\pi$.
 378 Thus, the phase relationship between ϕ_1 , ϕ_2 , and ϕ_3 is
 379 crucial. According to Eq. (29) only the term coming from
 380 the explicit phonon-phonon interaction, i.e., the second
 381 term on the rhs., will affect these phases. Neglecting the
 382 phonon-phonon interaction ϕ_1 , ϕ_2 , and ϕ_3 are indepen-
 383 dent of each other and chiral and standard CDWs are
 384 degenerate. So the particular form of $H_{\text{ph-ph}}$ is essential
 385 in order to obtain a chiral CDW.

386 C. Self-consistency equations

387 Proceeding further, we assume that the electron-
 388 phonon interaction constants are real, i.e., $\Phi_1 = \Phi_2 =$
 389 $\Phi_3 = 0$. Taking into account the symmetry of the con-
 390 duction bands and the equality of the electron-phonon
 391 interactions, we have $|\delta_{\mathbf{Q}1}| = |\delta_{\mathbf{Q}2}| = |\delta_{\mathbf{Q}3}| = |\delta_{\mathbf{Q}}|$ and
 392 $|\Delta_{\mathbf{Q}1}| = |\Delta_{\mathbf{Q}2}| = |\Delta_{\mathbf{Q}3}| = |\Delta_{\mathbf{Q}}|$. Therewith the free
 393 energy follows as

$$\begin{aligned} F &= \frac{1}{\beta N} \sum_{\mathbf{k}, \nu} \ln(1 - n_{\mathbf{k}\nu}) + \mu + \frac{3\hbar\omega}{4(g_{\mathbf{Q}})^2} |\delta_{\mathbf{Q}}|^2 \\ &- U_{fc} n_f \sum_{\alpha} n_{\alpha} - U_{cc} \sum_{\alpha} \sum_{\beta > \alpha} n_{\alpha} n_{\beta} + \frac{3}{U_{fc}} |\Delta_{\mathbf{Q}}|^2 \\ &+ \frac{4D}{g_{\mathbf{Q}}^4} |\delta_{\mathbf{Q}}|^4 \left[\cos(2\phi_1) \cos(2\phi_2) + \cos(2\phi_1) \cos(2\phi_3) \right. \\ &\left. + \cos(2\phi_2) \cos(2\phi_3) \right] + \frac{3\tilde{D}}{g_{\mathbf{Q}}^4} |\delta_{\mathbf{Q}}|^4, \end{aligned} \quad (31)$$

394 where $n_{\mathbf{k}\nu} = [1 + e^{\beta(E_{\mathbf{k}\nu} - \mu)}]^{-1}$. The quasiparticle en-
 395 ergies $E_{\mathbf{k}\nu}$ are obtained by diagonalizing the Hamilton
 396 matrix

$$[H] = \begin{pmatrix} \bar{\epsilon}_{\mathbf{k}f} & \tilde{\Delta}_{\mathbf{Q}1}^* & \tilde{\Delta}_{\mathbf{Q}2}^* & \tilde{\Delta}_{\mathbf{Q}3}^* \\ \tilde{\Delta}_{\mathbf{Q}1} & \bar{\epsilon}_{\mathbf{k}+\mathbf{Q}1} & 0 & 0 \\ \tilde{\Delta}_{\mathbf{Q}2} & 0 & \bar{\epsilon}_{\mathbf{k}+\mathbf{Q}2} & 0 \\ \tilde{\Delta}_{\mathbf{Q}3} & 0 & 0 & \bar{\epsilon}_{\mathbf{k}+\mathbf{Q}3} \end{pmatrix}. \quad (32)$$

397 Evidently the three conduction bands are coupled to
 398 each other via their coupling to the single valence band.
 399 The resulting quasiparticle band structure exhibits a gap,
 400 whose magnitude is determined by the squared modulus
 401 of the “gap parameter”

$$\tilde{\Delta}_{\mathbf{Q}\alpha} = \delta_{\mathbf{Q}\alpha} - \Delta_{\mathbf{Q}\alpha}. \quad (33)$$

402 Naturally the relation (30) maximizes the gap parameter
 403 $|\tilde{\Delta}_{\mathbf{Q}\alpha}|$ for every given $|\delta_{\mathbf{Q}\alpha}|$ and $|\Delta_{\mathbf{Q}\alpha}|$. On the other
 404 hand, $E_{\mathbf{k}\nu}$ depends, via $\cos(\theta_\alpha - \phi_\alpha)$, on the phase dif-
 405 ferences only, i.e., the quasiparticle band structure can
 406 not be used to fix the particular values of θ_1 , θ_2 , and θ_3 .
 407 We further note that $|\Delta_{\mathbf{Q}}| > 0$ if and only if $|\delta_{\mathbf{Q}}| > 0$. To
 408 elaborate let us first consider the case $g_{\mathbf{Q}} = 0$. In the EI
 409 phase ($|\Delta_{\mathbf{Q}}| > 0$) the system realizes a CDW. When $g_{\mathbf{Q}}$
 410 becomes finite in addition, the lattice adjusts commen-
 411 surate with the electron density modulation. Hence, in
 412 this case, any finite $g_{\mathbf{Q}}$ immediately results in $|\delta_{\mathbf{Q}}| > 0$.
 413 On the contrary, at vanishing Coulomb interaction but
 414 sufficiently large $g_{\mathbf{Q}} > g_{\mathbf{Q},c}$, a lattice instability devel-
 415 ops leading to a finite $\sum_{\mathbf{k}} (c_{\mathbf{k}+\mathbf{Q}_\alpha}^\dagger f_{\mathbf{k}})$. This hybridiza-
 416 tion parameter enters the explicit equation for the EI
 417 order parameter (12). $|\Delta_{\mathbf{Q}}| > 0$ then follows from any
 418 finite Coulomb interaction. Our approach therefore does
 419 not discriminate between an excitonic and phonon-driven
 420 instability if both electron-electron and electron-phonon
 421 interactions are at play.

422 We now relate $|\Delta_{\mathbf{Q}}|$ and $|\delta_{\mathbf{Q}}|$. Minimizing F , Eq. (31),
 423 with respect to θ_α yields the constraint (30). This entails
 424 that the gap parameter is given by $|\tilde{\Delta}_{\mathbf{Q}\alpha}| = |\delta_{\mathbf{Q}}| + |\Delta_{\mathbf{Q}}|$.
 425 Depending on the sign of D , a different phase relationship
 426 between ϕ_1 , ϕ_2 , and ϕ_3 will be favored. For $D > 0$ we
 427 find that one phase has to be a multiple of π and another
 428 phase must be an odd multiple of $\pi/2$. The third phase
 429 is arbitrary. In this case the considered phonon-phonon
 430 interaction introduces a fixed phase difference between
 431 the lattice distortion modes. That is, $\theta_1 \neq \theta_2 \neq \theta_3$, and
 432 we observe a chiral CDW. On the other hand, for $D < 0$,
 433 F takes its minimum if all phases are a multiple $\pi/2$. The
 434 resulting CDW is then nonchiral. For both cases ($D > 0$
 435 and $D < 0$), the free energy is minimized at finite values
 436 of $|\delta_{\mathbf{Q}}|$ if the constraint

$$\tilde{D} \geq 4|D| \quad (34)$$

437 is fulfilled. Since the experiments suggest a chiral CDW,
 438 we take $D > 0$. Without loss of generality we further set
 439 $\phi_1 = 0$, $\phi_2 = \pi/2$, $\phi_3 = 3\pi/10$, and assume $\tilde{D} = 4D$.
 440 The moduli of $|\delta_{\mathbf{Q}}|$ and $|\Delta_{\mathbf{Q}}|$ are then determined by
 441 $\partial F/\partial|\delta_{\mathbf{Q}}| = 0$ and $\partial F/\partial|\Delta_{\mathbf{Q}}| = 0$, respectively. Straight-
 442 forward calculation gives

$$\begin{aligned} \frac{3}{U_{fc}} |\Delta_{\mathbf{Q}}| &= \frac{3\hbar\omega}{4g_{\mathbf{Q}}^2} |\delta_{\mathbf{Q}}| + 8 \frac{D}{g_{\mathbf{Q}}^4} |\delta_{\mathbf{Q}}|^3 \left[\cos(2\phi_1) \cos(2\phi_2) \right. \\ &\quad \left. + \cos(2\phi_1) \cos(2\phi_3) + \cos(2\phi_2) \cos(2\phi_3) \right] \\ &\quad + 6 \frac{\tilde{D}}{g_{\mathbf{Q}}^4} |\delta_{\mathbf{Q}}|^3. \end{aligned} \quad (35)$$

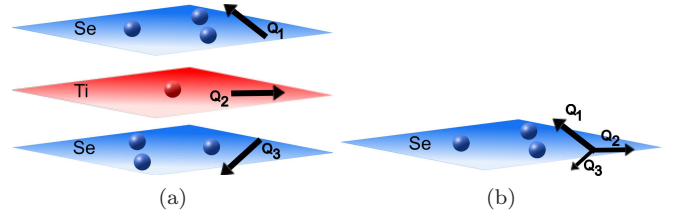
443 Let us finally stress that we can only specify values
 444 for the phases θ_α and ϕ_α . Which particular phase takes
 445 one of these values remains open. For instance, the sim-
 446 ultaneous transformations $\theta_2 \rightarrow \theta_3$ and $\phi_2 \rightarrow \phi_3$ do
 447 not change the free energy, but convert a clockwise chiral
 448 CDW in an anticlockwise one. The degeneracy of
 449 these two CDW states is in accord with the experimental
 450 findings for 1T-TiSe₂.⁵

451 D. Characterization of the CDW state in 1T-TiSe₂

452 Experiments identify a close connection between the
 453 appearance of the CDW state and the periodic lattice dis-
 454 placement in 1T-TiSe₂.⁷ In the scheme developed in the
 455 preceding sections the CDW is directly accompanied by
 456 a lattice distortion. There the j -component ($j = x, y, z$)
 457 of the lattice deformation caused by the phonon α is

$$\tilde{u}_j^\alpha(\mathbf{r}) = \frac{1}{\sqrt{N}} \sum_l \sqrt{\frac{2\hbar}{\omega M_l}} |b_{\mathbf{Q}\alpha}^\dagger| \epsilon_{l,j}(\mathbf{Q}_\alpha) \cos(\mathbf{Q}_\alpha \mathbf{r} - \phi_{b\alpha}), \quad (36)$$

458 where $\epsilon_{l,j}(\mathbf{Q}_\alpha)$ is the j -component of the polarization
 459 vector, l labels the atoms in the unit cell, and M_l is the
 460 mass of the atom l . Clearly each CDW component α
 461 produces a 3D lattice distortion. Since $\phi_{b1} \neq \phi_{b2} \neq \phi_{b3}$
 462 if $\phi_1 \neq \phi_2 \neq \phi_3$, the lattice will be differently affected by
 463 the phonons \mathbf{Q}_1 , \mathbf{Q}_2 , and \mathbf{Q}_3 . Of course the lattice defor-
 464 mation by the phonon mode \mathbf{Q}_α is position-dependent; in
 465 this way a complicated distortion pattern of the ions can
 466 occur. An instructive picture can be achieved, however,
 467 if one neglects the \mathbf{r} -dependence in the xy -plane. In this
 468 simplified situation, depending on the z -component as a
 469 function of \mathbf{r} , the magnitude of the lattice displacement
 470 differs along \mathbf{Q}_1 , \mathbf{Q}_2 , and \mathbf{Q}_3 . As a result the differ-
 471 ent ionic layers of 1T-TiSe₂ are dominated by different
 472 phonon modes.⁷ The situation where the lower Se-ion
 473 layer is largely affected by the phonon mode \mathbf{Q}_3 , the Ti-
 474 ion layer by phonons with momentum \mathbf{Q}_2 , and the up-
 475 per Se-ion layer by the \mathbf{Q}_1 phonon mode, is illustrated
 476 schematically in Fig. 5(a). Let us consider the upper



477 FIG. 5. (color online) (a) For a chiral ordering the maximum
 478 lattice distortion due to the phonon \mathbf{Q}_α may be located in
 479 different ionic layers. (b) The Se ions in the upper layer are
 480 differently affected by the phonons having momentum \mathbf{Q}_1 ,
 \mathbf{Q}_2 , or \mathbf{Q}_3 . For further discussion see text.

478 plane of Se ions, which is analyzed in scanning tunneling
 479 microscopy experiments.⁵ There a relative difference of
 480

the phases $\phi_{b\alpha}$ leads, e.g., to a stronger displacement of the ions in the direction of \mathbf{Q}_1 than in the direction of \mathbf{Q}_2 and \mathbf{Q}_3 [see Fig. 5(b)]. Then the CDW transition can be viewed as a formation of “virtual layers” with ordering vectors assigned to a helical structure.⁵ The described distortion scenario equates with a fixed phase difference. Thereby the only crucial parameters are ϕ_1 , ϕ_2 , and ϕ_3 ; the finite z -component of the ordering vectors is not a required prerequisite for the chiral CDW.

We add that in our model both CDW transitions appear simultaneously, i.e., $T_{\text{CDW}} = T_{\text{chiral}}$. This contradicts the result $T_{\text{chiral}} < T_{\text{CDW}}$ by van Wezel.^{7,8} In that Landau-Ginzburg approach terms of second and quartic order in the order parameter appear. While the second-order term favors equal phases, the quartic-order term supports a phase difference.⁷ Hence there is a competition between a nonchiral and a chiral CDW state. This competition is absent in our approach where we have only a single term that fixes the values of ϕ_1 , ϕ_2 , ϕ_3 respectively θ_1 , θ_2 , θ_3 . Very recent X-ray diffraction and electrical transport measurements provide some evidence that the transition to the chiral CDW takes place at lower temperature than the CDW transition.⁵⁰ The difference between T_{CDW} and T_{chiral} is less than ten Kelvin however. Having disregarded fluctuation corrections, which are known to play an important role in the vicinity of a phase transition, we can not conclusively resolve this issue.

III. NUMERICAL RESULTS

A. Model assumptions

In view of the quasi-2D crystallographic and electronic structure of $1T$ -TiSe₂, and in order to simplify the numerics, we restrict the following analysis to a strictly 2D setting. Moreover, being close to the Fermi energy, we will approximate the bands parabolically¹⁰

$$\varepsilon_{\mathbf{k}f} = -t_f (k_x^2 + k_y^2), \quad (37)$$

$$\varepsilon_{\mathbf{k}1} = t_c^x (k_x - Q_{1x})^2 + t_c^y (k_y - Q_{1y})^2 + E_c, \quad (38)$$

with hopping amplitudes t_f , t_c^x , and t_c^y . The other two conduction bands $\varepsilon_{\mathbf{k}2}$ and $\varepsilon_{\mathbf{k}3}$ have analogous dispersions, but the momenta are rotated by $2\pi/3$ and $4\pi/3$, respectively. All three conduction bands share the same minimum E_c , see Fig. 3.

From the band dispersion provided by Monney *et al.* in Ref. 10 we derive $t_f = 1.3$ eV, which will be taken as the unit of energy hereafter, and $t_c^x = 0.042$ and $t_c^y = 0.105$. The bare phonon frequency is estimated as $\hbar\omega = 0.013$, in accordance with the value given by Weber *et al.* in Ref. 20. Furthermore, we set $E_c = -3.30$ and $U_{cc} = U_{fc} + 1.0$. For the phonon-phonon interaction constant we take $D = 10^{-4}$.

The self-consistency loop, comprising the determination of the EI order parameter, the static lattice distortion, the total and partial particle densities and the

chemical potential, is solved iteratively until the relative error of each physical quantity is less than 10^{-6} . The numerical integrations were performed using the Cubpack package.⁵¹

B. Phase diagram of the mEFKM

To set the stage for the analysis of the interplay of Coulomb and electron-phonon interaction effects we first discuss the phase diagram of the pure mEFKM, cf. Fig. 6. Here, since $g_{\mathbf{Q}} = 0$ (and as a result $\delta_{\mathbf{Q}\alpha} = 0$), the EI low-temperature phase typifies a normal CDW. As for the EFKM on a square lattice (see inset), at $T = 0$ we find a finite critical Coulomb strength above which the EI phase does not exist. This is because the large band splitting caused by the Hartree term of the Coulomb interaction prevents c - f electron coherence.⁴² In contrast

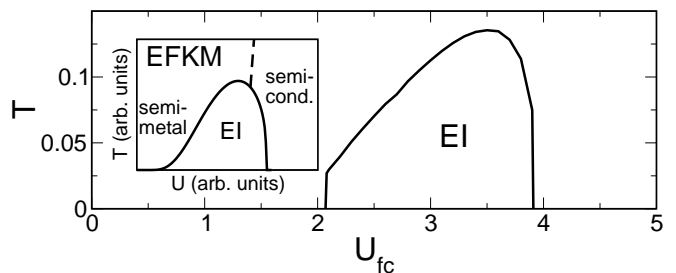


FIG. 6. Phase diagram of the mEFKM. The inset displays the schematic phase diagram of the simplified two-band EFKM on a square lattice according to Ref. 42.

to the EFKM, in our four-band model we also find a critical lower Coulomb strength for the EI phase. This can be understood as follows: since the valence band is isotropic while the conduction-band dispersions are strongly anisotropic, particles close to the Fermi level do not find a large number of partners with appropriate momentum for electron-hole pairing. Thus, for U_{fc} smaller than a critical Coulomb attraction, the amount of energy to create a macroscopic number of excitons is larger than the energy gain from the condensation transition into the EI state. Therefore the system remains in the semimetallic phase.⁵² The rather abrupt increase of the critical temperature at the lower critical Coulomb interaction is due to the degeneracy of the conduction bands and the particular anisotropy used.

C. Influence of the lattice degrees of freedom

We now analyze the situation when phonons participate in the CDW formation. In Fig. 7 we consider the dependence of the EI order parameter $|\Delta_{\mathbf{Q}}|$ and the static lattice distortion $|\delta_{\mathbf{Q}}|$ on the interaction constants at $T = 0$. For small electron-phonon coupling the behavior of the EI order parameter resembles the situation for the mEFKM (EI limit). Differences appear for

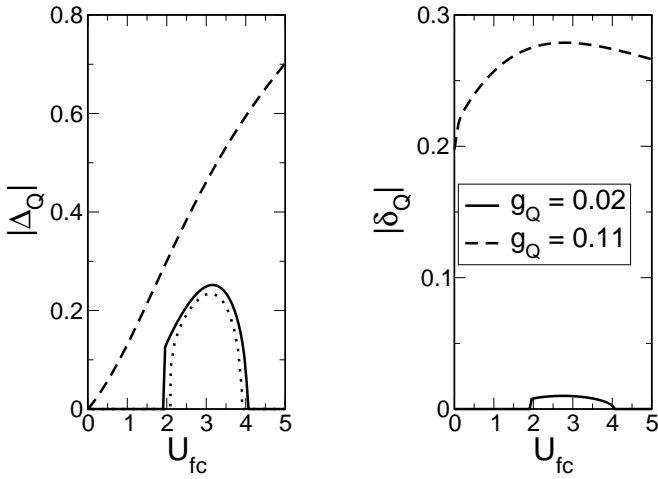


FIG. 7. EI order parameter $|\Delta_{\mathbf{Q}}|$ (left panel) and static lattice distortion $|\delta_{\mathbf{Q}}|$ (right panel) as a function of the Coulomb interaction U_{fc} at $T = 0$. Results are given for $g_{\mathbf{Q}} = 0.02$ (solid lines) and $g_{\mathbf{Q}} = 0.11$ (dashed lines). For comparison, in the left-hand panel, the EI order parameter of the pure mEFKM is included ($g_{\mathbf{Q}} = 0$; dotted line).

573 $g_{\mathbf{Q}} = 0.11$ where we do not find a lower critical U_{fc} for
 574 the CDW phase, i.e., now any finite U_{fc} leads to a finite
 575 $|\Delta_{\mathbf{Q}}|$. The order parameter $|\Delta_{\mathbf{Q}}|$ shows an almost linear
 576 dependence on U_{fc} , which means that the electron-hole
 577 pairing probability ($\propto |\Delta_{\mathbf{Q}}|/U_{fc}$) remains approximately
 578 constant. The tendency towards exciton formation and
 579 condensation is notably enhanced as $g_{\mathbf{Q}}$ increases at fixed
 580 U_{fc} . The static lattice distortion is tiny and follows the
 581 behavior of the EI order parameter for small $g_{\mathbf{Q}}$. For
 582 $g_{\mathbf{Q}} = 0.11$ we observe a non-monotonic behavior of $|\delta_{\mathbf{Q}}|$
 583 as a function of the electron-electron interaction. At
 584 very large electron-phonon couplings the influence of the
 585 electron-electron interaction on $|\delta_{\mathbf{Q}}|$ weakens (not shown
 586 in Fig. 7).

587 Figure 8 gives the dependence of the order param-
 588 eters on the electron-phonon coupling constant at fixed
 589 U_{fc} . For $U_{fc} = 2.5$ the order parameters remain finite
 590 as $g_{\mathbf{Q}} \rightarrow 0$ since we already have a CDW in the pure
 591 mEFKM (see Fig. 6). A Coulomb strength $U_{fc} = 5.0$, on
 592 the other hand, does not lead to an EI if phonons are ab-
 593 sent. Then we find a lower critical $g_{\mathbf{Q}}$. Furthermore we
 594 observe a saturation of the EI order parameter with in-
 595 creasing $g_{\mathbf{Q}}$, since $|\Delta_{\mathbf{Q}}|$ is limited by the number of elec-
 596 trons that can participate in the electron-hole pairing.
 597 Within our approximation the expectation value of the
 598 phonon-creation operator is not bounded and $|\delta_{\mathbf{Q}}|$ con-
 599 tinuously increases with enhanced electron-phonon cou-
 600 pling. Note that an increasing phonon-phonon inter-
 601 action strength D reduces the static lattice distortion
 602 and therefore leads to a smaller EI order parameter (not
 603 shown).
 604

605 Finite temperature effects are illustrated in Fig. 9. For
 606 very small electron-phonon coupling the phase diagram
 607 again resembles the situation for the mEFKM. As the

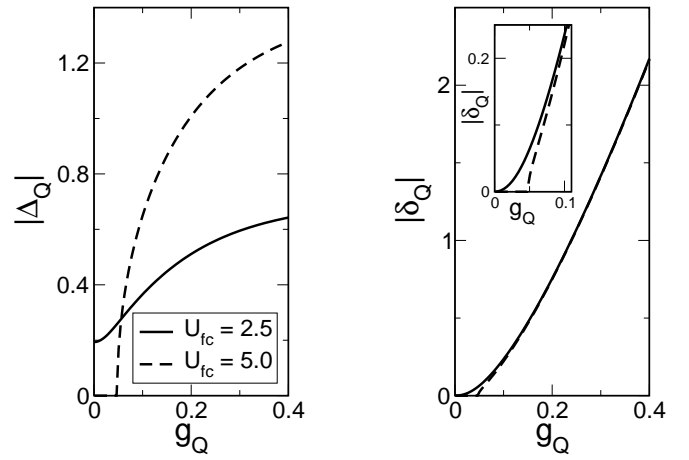


FIG. 8. EI order parameter $|\Delta_{\mathbf{Q}}|$ (left panel) and static lattice distortion $|\delta_{\mathbf{Q}}|$ (right panel) as a function of the electron-phonon coupling $g_{\mathbf{Q}}$ at $T = 0$. Results are given for $U_{fc} = 2.5$ (solid lines) and $U_{fc} = 5.0$ (dashed lines). The right-hand inset enlarges the region of small $g_{\mathbf{Q}}$.

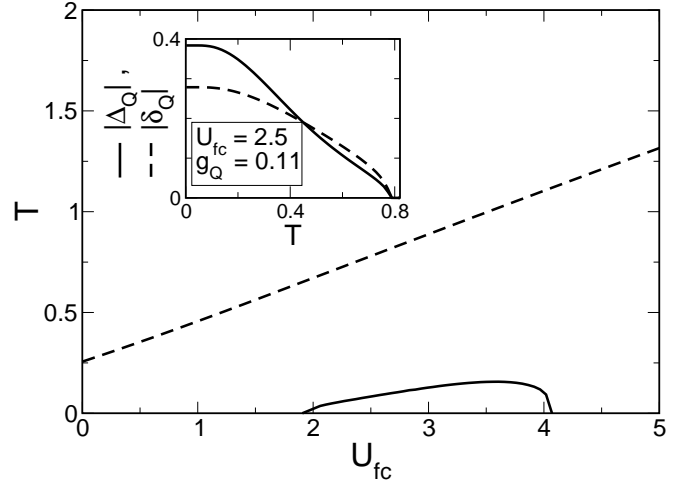


FIG. 9. CDW phase boundaries for $g_{\mathbf{Q}} = 0.02$ (solid line) and $g_{\mathbf{Q}} = 0.11$ (dashed line). The inset gives the EI order parameter (solid line) and the static lattice distortion (dashed line) as a function of temperature for $g_{\mathbf{Q}} = 0.11$ at $U_{fc} = 2.5$.

609 interaction strength $g_{\mathbf{Q}}$ increases the situation changes
 610 dramatically. For sufficiently large electron-phonon cou-
 611 plings, we no longer find critical lower and upper val-
 612 ues U_{fc} for the CDW transition and the transition tem-
 613 perature increases linearly with U_{fc} . That is the criti-
 614 cal temperature is significantly enhanced by $g_{\mathbf{Q}}$. Obvi-
 615 ously electron-hole attraction and electron-phonon cou-
 616 pling act together in the formation of a very stable CDW
 617 phase. The inset shows how the order parameters are
 618 suppressed by increasing temperature. Here the static
 619 lattice distortion reveals a typical mean-field dependence.

620 Our findings are summarized by the ground-state
 621 phase diagram shown in Fig. 10. For weak electron-
 622 phonon couplings $g_{\mathbf{Q}}$ the CDW is mainly driven by the

623 Coulomb attraction U_{fc} between electrons and holes. 624 The greater $g_{\mathbf{Q}}$, the larger the region where the CDW 625 is stable. For $g_{\mathbf{Q}} > 0.09$ the electron-phonon coupling 626 alone can cause the CDW transition, even at $U_{fc} = 0$ 627 (blue line in Fig. 10). The CDW is chiral in this limit, 628 whereas the CDW in the opposite EI limit does not ex- 629 hibit chirality ($g_{\mathbf{Q}} = 0$, red line in Fig. 10).

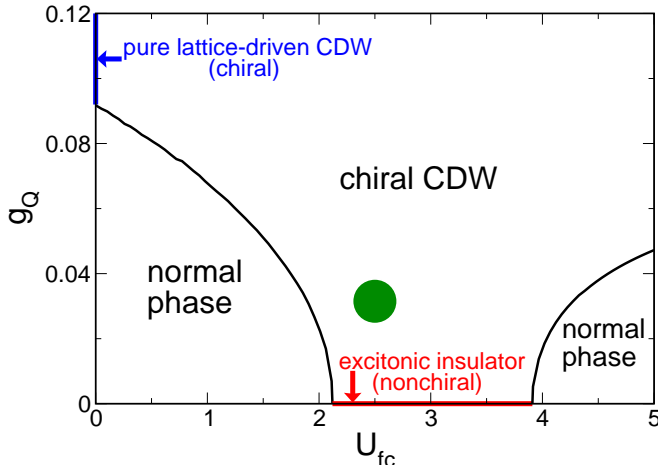


FIG. 10. (color online) Ground-state phase diagram of the mEFKM with additional electron-phonon coupling. The CDW phase is characterized by a finite gap parameter $|\tilde{\Delta}_{\mathbf{Q}}|$. The red line at $g_{\mathbf{Q}} = 0$ marks the EI phase of the pure mEFKM. The blue line at $U_{fc} = 0$ refers to a CDW induced solely by the electron-lattice interaction. The green point designates the range of model parameters appropriate for $1T$ -TiSe₂.

D. Relation to $1T$ -TiSe₂

633 Based on the phase diagram derived for the mEFKM 634 with electron-phonon coupling, we now attempt to es- 635 timate the electron-electron and electron-phonon inter- 636 action constants, U_{fc} and $g_{\mathbf{Q}}$, for $1T$ -TiSe₂. To make 637 contact with the experiments we take the displacements 638 of the Ti ions measured by Di Salvo *et al.*: $\tilde{u}_{l=\text{Ti}} = 0.04\text{\AA}$ 639 with $\tilde{u} = \sum_l \tilde{u}_l$.⁴ Then, from Eq. (36), we can specify the 640 value of $|\langle b_{\mathbf{Q}}^\dagger \rangle|$. For $1T$ -TiSe₂, the gap parameter was de- 641 termined experimentally as 120 meV by Monney *et al.*, 642 cf. Ref. 44. Adjusting this value to our theoretical re- 643 sults yields $U_{fc} \approx 2.5$ (≈ 3 eV) and $g_{\mathbf{Q}} \approx 0.03$ (≈ 0.04 644 eV); see the green marker in Fig. 10. For these values 645 both the theoretical ion displacement and gap param- 646 eter are in the same order of magnitude as the measured 647 ones. Using $U_{fc} \approx 2.5$ for $1T$ -TiSe₂, the electron-hole 648 pairing is BCS-like. Since $g_{\mathbf{Q}} \simeq 0.03$ is too small to 649 cause a CDW for vanishing Coulomb interaction and, as 650 discussed above, the EI scenario alone will not yield a 651 stable chiral CDW, our results are in favor of a combined 652 lattice-deformation/EI mechanism for the experimentally 653 observed chiral CDW transition, as suggested in Refs. 22

IV. CONCLUSIONS

654 and 53. 655
656 In this work we have argued how the chiral charge- 657 density-wave (CDW) phase in $1T$ -TiSe₂ may be sta- 658 bilized. In the framework of the multiband extended 659 Falicov-Kimball model (mEFKM) we showed that a 660 purely electronic—exciton pairing and condensation— 661 mechanism is insufficient to induce the observed (long- 662 ranged) chiral charge order. We propose that the cou- 663 pling of the electrons to the lattice degrees of freedom is 664 essential for the formation of a chiral CDW state. In par- 665 ticular, an explicit phonon-phonon interaction between 666 the phonons that become soft at the critical temperature 667 has to be taken into account in order to stabilize the chi- 668 ral CDW. We note that in our model clockwise and anti- 669 clockwise CDWs are degenerate. This is in accord with 670 experimental findings.⁵ The chiral property can properly 671 be observed in the ionic displacements accompanying the 672 CDW in $1T$ -TiSe₂.

673 Concerning the microscopic mechanism underlying the 674 CDW transition, we demonstrated that electron-electron 675 interaction and electron-phonon coupling support each 676 other in driving the electron-hole pairing and finally the 677 instability. This suggests that the CDW transition in 678 $1T$ -TiSe₂ is due to a combined lattice distortion and 679 exciton-condensation effect. The outcome is a spon- 680 taneous broken-symmetry CDW low-temperature state 681 with small but finite lattice deformation. Of course, both 682 the mean-field treatment of the Coulomb interaction and 683 the frozen-phonon approach are rather crude approxima- 684 tions and a more elaborated study of the complex in- 685 terplay between the electronic and phononic degrees of 686 freedom is highly desirable to confirm our proposed sce- 687 nario for the chiral CDW transition in $1T$ -TiSe₂.

688 Let us finally point out that we called $|\Delta_{\mathbf{Q}}|$ the 689 excitonic-insulator order parameter on account of its ana- 690 log in the EFKM.^{35–42} The meaning of a finite $|\Delta_{\mathbf{Q}}|$ in 691 the presence of a band coupling is imprecise however. 692 Likewise a spontaneous hybridization of the valence band 693 with one of the conduction bands, signaling the exciton 694 condensate in the mEFKM, may be induced by a suf- 695 ficiently large electron-phonon coupling. A general cri- 696 terion for the formation of an exciton condensate in a 697 strongly coupled band situation has not been established 698 so far. This is an open issue which deserves further anal- 699 ysis because of its relevance in characterizing the nature 700 of CDW transitions also in other materials.^{54,55}

ACKNOWLEDGMENTS

701 We thank P. Aebi, K. W. Becker, F. X. Bronold, 702 D. Ihle, G. Monney, and P. V. Nham for valuable 703 discussions. This work is supported by the Deutsche 704 Forschungsgemeinschaft through SFB 652 (project B5), 705

706 by the Fonds National Suisse pour la Recherche Scien- 709
 707 tifique through Div. II, the Swiss National Center of 710
 708 Competence in Research MaNEP, and the U.S. Depart- 711
 ment of Energy. C.M. acknowledges also support by the
 Fonds National Suisse pour la Recherche Scientifique un-
 der grant PA00P2-142054.

-
- 712 ¹ R. Peierls, *Quantum theory of solids* (Oxford University 768
 713 Press, Oxford, 1955).
 714 ² J. Sólyom, *Adv. Phys.* **28**, 201 (1979).
 715 ³ G. Grüner, *Density Waves in Solids* (Perseus Publishing, 769
 716 2000).
 717 ⁴ F. J. Di Salvo, D. E. Moncton, and J. V. Waszczak, *Phys.* 770
 718 *Rev. B* **14**, 4321 (1976).
 719 ⁵ J. Ishioka, Y. H. Liu, K. Shimatake, T. Kurosawa, 771
 720 K. Ichimura, Y. Toda, M. Oda, and S. Tanda, *Phys. Rev.* 772
 721 *Lett.* **105**, 176401 (2010).
 722 ⁶ J. van Wezel and P. Littlewood, *Physics* **3**, 87 (2010).
 723 ⁷ J. van Wezel, *Europhys. Lett.* **96**, 67011 (2011).
 724 ⁸ J. van Wezel, *Physica B* **407**, 1779 (2012).
 725 ⁹ H. Cercellier, C. Monney, F. Clerc, C. Battaglia, L. De- 773
 726 spont, M. G. Garnier, H. Beck, P. A. ans L. Patthey, 774
 727 H. Berger, and L. Forró, *Phys. Rev. Lett.* **99**, 146403 775
 728 (2007).
 729 ¹⁰ C. Monney, H. Cercellier, F. Clerc, C. Battaglia, E. F. 776
 730 Schwier, C. Didiot, M. G. Garnier, H. Beck, P. Aebi, 777
 731 H. Berger, L. Forró, and L. Patthey, *Phys. Rev. B* **79**, 778
 732 045116 (2009).
 733 ¹¹ C. Monney, C. Battaglia, H. Cercellier, P. Aebi, and 779
 734 H. Beck, *Phys. Rev. Lett.* **106**, 106404 (2011).
 735 ¹² M. M. May, C. Brabetz, C. Janowitz, and R. Manzke, 780
 736 *Phys. Rev. Lett.* **107**, 176405 (2011).
 737 ¹³ T. Rohwer, S. Hellmann, M. Wiesenmayer, C. Sohr, 781
 738 A. Stange, B. Slomski, A. Carr, Y. Liu, L. M. Avila, 782
 739 M. Kalläne, S. Mathias, L. Kipp, K. Rossnagel, and 783
 740 M. Bauer, *Nature* **471**, 490 (2011).
 741 ¹⁴ H. P. Hughes, *J. Phys. C* **10**, L319 (1977).
 742 ¹⁵ K. Rossnagel, L. Kipp, and M. Skibowski, *Phys. Rev. B* 784
 743 **65**, 235101 (2002).
 744 ¹⁶ Y. Yoshida and K. Motizuki, *J. Phys. Soc. Japan* **49**, 898 785
 745 (1980).
 746 ¹⁷ K. Motizuki, N. Suzuki, Y. Yoshida, and Y. Takaoka, *Solid* 786
 747 *State Commun.* **40**, 995 (1981).
 748 ¹⁸ N. Suzuki, A. Yamamoto, and K. Motizuki, *J. Phys. Soc.* 787
 749 *Japan* **54**, 4668 (1985).
 750 ¹⁹ M. Holt, P. Zschack, H. Hong, M. Y. Chou, and T. C. 788
 751 Chiang, *Phys. Rev. Lett.* **86**, 3799 (2001).
 752 ²⁰ F. Weber, S. Rosenkranz, J.-P. Castellan, R. Osborn, 789
 753 G. Karapetrov, R. Hott, R. Heid, K.-P. Bohnen, and 790
 754 A. Alatas, *Phys. Rev. Lett.* **107**, 266401 (2011).
 755 ²¹ M. Calandra and F. Mauri, *Phys. Rev. Lett.* **106**, 196406 791
 756 (2011).
 757 ²² J. van Wezel, P. Nahai-Williamson, and S. S. Saxena, 792
 758 *Europhys. Lett.* **89**, 47004 (2010).
 759 ²³ C. Monney, G. Monney, P. Aebi, and H. Beck, *New J.* 793
 760 *Phys.* **14**, 075026 (2012).
 761 ²⁴ J. Neuenschwander and P. Wachter, *Phys. Rev. B* **41**, 794
 762 12693 (1990).
 763 ²⁵ P. Wachter and B. Bucher, *Physica B* **408**, 51 (2013).
 764 ²⁶ K. Kanda, K. Machida, and T. Matsubara, *Solid State* 795
 765 *Commun.* **19**, 651 (1976).
 766 ²⁷ T. Portengen, T. Östreich, and L. J. Sham, *Phys. Rev.* 796
 767 *Lett.* **76**, 3384 (1996).
 768 ²⁸ C. D. Batista, *Phys. Rev. Lett.* **89**, 166403 (2002).
 769 ²⁹ N. F. Mott, *Philos. Mag.* **6**, 287 (1961).
 770 ³⁰ R. Knox, in *Solid State Physics*, edited by F. Seitz and 771
 772 D. Turnbull (Academic Press, New York, 1963) p. Suppl. 773
 774 5 p. 100.
 775 ³¹ D. Jérôme, T. M. Rice, and W. Kohn, *Physical Review* 774
 775 **158**, 462 (1967).
 776 ³² F. X. Bronold and H. Fehske, *Phys. Rev. B* **74**, 165107 775
 776 (2006).
 777 ³³ C. D. Batista, J. E. Gubernatis, J. Bonča, and H. Q. Lin, 776
 778 *Phys. Rev. Lett.* **92**, 187601 (2004).
 779 ³⁴ P. Farkašovský, *Phys. Rev. B* **77**, 155130 (2008).
 780 ³⁵ C. Schneider and G. Czycholl, *Eur. Phys. J. B* **64**, 43 777
 781 (2008).
 782 ³⁶ D. Ihle, M. Pfafferoth, E. Burovski, F. X. Bronold, and 778
 783 H. Fehske, *Phys. Rev. B* **78**, 193103 (2008).
 784 ³⁷ B. Zenker, D. Ihle, F. X. Bronold, and H. Fehske, *Phys.* 779
 785 *Rev. B* **81**, 115122 (2010).
 786 ³⁸ V.-N. Phan, K. W. Becker, and H. Fehske, *Phys. Rev. B* 780
 787 **81**, 205117 (2010).
 788 ³⁹ B. Zenker, D. Ihle, F. X. Bronold, and H. Fehske, *Phys.* 781
 789 *Rev. B* **83**, 235123 (2011).
 790 ⁴⁰ V.-N. Phan, H. Fehske, and K. W. Becker, *Europhys. Lett.* 782
 791 **95**, 17006 (2011).
 792 ⁴¹ K. Seki, R. Eder, and Y. Ohta, *Phys. Rev. B* **84**, 245106 783
 793 (2011).
 794 ⁴² B. Zenker, D. Ihle, F. X. Bronold, and H. Fehske, *Phys.* 784
 795 *Rev. B* **85**, 121102R (2012).
 796 ⁴³ C. Monney, E. F. Schwier, M. G. Garnier, N. Mariotti, 785
 797 C. Didiot, H. Cercellier, J. Marcus, H. Berger, A. N. Titov, 786
 798 H. Beck, and P. Aebi, *New J. Phys.* **12**, 125019 (2010).
 799 ⁴⁴ C. Monney, E. F. Schwier, M. G. Garnier, N. Mariotti, 787
 800 C. Didiot, H. Beck, P. Aebi, C. Cercellier, J. Marcus, 788
 801 C. Battaglia, H. Berger, and A. N. Titov, *Phys. Rev. B* 789
 802 **81**, 155104 (2010).
 803 ⁴⁵ M. Cazzaniga, H. Cercellier, M. Holzmann, C. Monney, 790
 804 P. Aebi, G. Onida, and V. Olevano, *Phys. Rev. B* **85**, 791
 805 195111 (2012).
 806 ⁴⁶ C. Monney, G. Monney, P. Aebi, and H. Beck, *Phys. Rev.* 792
 807 *B* **85**, 235150 (2012).
 808 ⁴⁷ H. Ehrenreich and A. W. Overhauser, *Phys. Rev.* **104**, 331 793
 809 (1956).
 810 ⁴⁸ J. M. Ziman, *Electrons and Phonons* (Clarendon, London, 794
 811 1960).
 812 ⁴⁹ N. W. Ashcroft and N. D. Mermin, *Solid state physics* 795
 813 (Saunders College Publ. Philadelphia, 1976).
 814 ⁵⁰ J.-P. Castellan, S. Rosenkranz, R. Osborn, Q. Li, K. Gray, 796
 815 G. Karapetrov, J. Ruff, and J. van Wezel, (2012), 797
 816 preprint.
 817 ⁵¹ R. Cools and A. Haegemans, *ACM Transactions on Math-* 798
 818 *ematical Software* **29**, 287 (2003).
 819 ⁵² J. Zittartz, *Phys. Rev.* **162**, 752 (1967).
 820 ⁵³ Z. Zhu, Y. Cheng, and U. Schwingenschlögl, *Phys. Rev.* 799
 821 *B* **85**, 245133 (2012).
 822 ⁵⁴ T. Kaneko, T. Toriyama, T. Konishi, and Y. Ohta, (2012), 800
 823 preprint.

⁸²⁴ ⁵⁵ D. K. Efimkin, Y. E. Lozovik, and A. A. Sokolik, (2012), ⁸²⁵ preprint.